THE JOURNAL OF BIOLOGICAL CHEMISTRY VOL. 291, NO. 36, pp. 18620–18631, September 2, 2016

Heat Shock Protein 90 kDa (Hsp90) Has a Second Functional Interaction Site with the Mitochondrial Import Receptor Tom70*[S]

Received for publication, December 12, 2015, and in revised form, July 7, 2016 Published, JBC Papers in Press, July 8, 2016, DOI 10.1074/jbc.M115.710137

Leticia M. Zanphorlin[‡1], Tatiani B. Lima[‡1], Michael J. Wong[§], Tiago S. Balbuena[¶], Conceição A. S. A. Minetti[‖], David P. Remeta[‖], Jason C. Young[§2], Leandro R. S. Barbosa[**], Fabio C. Gozzo[‡], and Carlos H. I. Ramos[‡3]

From the [‡]Institute of Chemistry, University of Campinas UNICAMP, Campinas SP, 13083-970, Brazil, the [§]Department of Biochemistry, McGill University, Groupe de Recherche Axé sur la Structure des Protéines, Montreal, QC H3G 0B1, Canada, the [¶]College of Agricultural and Veterinary Sciences, State University of Sao Paulo, Jaboticabal, Sao Paulo, 14884-900 Brazil, the [‖]Department of Chemistry and Chemical Biology, Rutgers, The State University of New Jersey, Piscataway, New Jersey 08854, and the [**]Instituto de Fisica, Universidade de Sao Paulo USP, Sao Paulo SP, 05508-090 Brazil

To accomplish its crucial role, mitochondria require proteins that are produced in the cytosol, delivered by cytosolic Hsp90, and translocated to its interior by the translocase outer membrane (TOM) complex. Hsp90 is a dimeric molecular chaperone and its function is modulated by its interaction with a large variety of co-chaperones expressed within the cell. An important family of co-chaperones is characterized by the presence of one TPR (tetratricopeptide repeat) domain, which binds to the C-terminal MEEVD motif of Hsp90. These include Tom70, an important component of the TOM complex. Despite a wealth of studies conducted on the relevance of Tom70·Hsp90 complex formation, there is a dearth of information regarding the exact molecular mode of interaction. To help fill this void, we have employed a combined experimental strategy consisting of cross-linking/mass spectrometry to investigate binding of the C-terminal Hsp90 domain to the cytosolic domain of Tom70. This approach has identified a novel region of contact between C-Hsp90 and Tom70, a finding that is confirmed by probing the corresponding peptides derived from cross-linking experiments via isothermal titration calorimetry and mitochondrial import assays. The data generated in this study are combined to input constraints for a molecular model of the Hsp90/Tom70 interaction, which has been validated by small angle x-ray scattering, hydrogen/deuterium exchange, and mass spectrometry. The resultant model suggests that only one of the MEEVD motifs within dimeric Hsp90 contacts Tom70. Collectively, our findings provide significant insight on the mechanisms by which preproteins interact with Hsp90 and are translocated via Tom70 to the mitochondria.

The mitochondrion is involved in a number of critical cellular processes including metabolism and iron homeostasis. This organelle requires different proteins to accomplish its crucial role within the cell, most of which are produced in the cytosol and must be translocated to the mitochondrial interior to fulfill their functions (1). One major translocation pathway involves the heat shock protein 90 kDa (Hsp90) that binds and delivers unfolded proteins (preproteins) to the translocase of the outer mitochondrial membrane (TOM)[4] complex (2).

Hsp90 is a ubiquitous and essential molecular chaperone required for the folding and activation of a broad array of protein substrates (*i.e.* clients) in eukaryotes. The chaperone functions as a homodimer via high-affinity dimerization of the C-terminal domain (3–6). Hsp90 modulates complex physiological and pathophysiological processes such as development and differentiation, acts as a capacitor of phenotypic evolution, and assumes an important role in a number of diseases including cancer and neurodegeneration. Given its critical physiological role, Hsp90 is one of the most abundant proteins in the cytosol of eukaryotes and is responsible for activation of ~10% of the yeast proteome. Hsp90 consists of two polypeptide chains, each monomer comprised of three domains designated as N, M, and C. The N-terminal domain contains a nucleotide binding site and is connected via a charged linker region to the M-domain, which is critical to substrate binding. The C-terminal domain (residues 566–732 in the human α-isoform) includes a dimerization interface comprised of residues 652–671, and encompasses the MEEVD motif (residues 728–732), which is recognized as a TPR co-chaperone interaction site (7–9) as described below.

The TOM complex possesses two membrane import receptors, designated as Tom20 and Tom70. The latter is an Hsp90 co-chaperone that associates to form a high affinity complex with a monomer:dimer stoichiometry (10). Tom70 contains at least seven tetratricopeptide repeat (TPR) domains in its cyto-

* This work was supported in part by Fundação de Amparo à Pesquisa do Estado de São Paulo Grant FAPESP 2012/50161-8, Ministério da Ciência e Tecnologia/Conselho Nacional de Desenvolvimento Científico e Tecnológico (MCT/CNPq), and fellowships from FAPESP and the Canadian Institutes of Health Research (MOP-130332). The authors declare they have no conflict of interest with the contents of this article.
[S] This article contains supplemental Figs. S1 and S2 and Videos S1–S5.
[1] Both authors contributed equally to the results of this work.
[2] Holds a Canada Research Chair in Molecular Chaperones.
[3] Supported by INBEB (Instituto Nacional de Biologia Estrutural e Bioimagem). To whom correspondence should be addressed. Tel.: 55-19-35213001; Fax: 55-19-35213023; E-mail: cramos@iqm.unicamp.br.

[4] The abbreviations used are: TOM, translocase of the mitochondria outer membrane; C-Hsp90, the C-terminal domain of heat shock protein 90 kDa; DSS, disuccinimidyl suberate; HDX, hydrogen/deuterium exchange; Hsp, heat shock protein; ITC, isothermal titration calorimetry; TPR, tetratricopeptide repeat; SAXS, small angle x-ray scattering; XL-MS, cross-linking/mass spectrometry assay; PDB, Protein Data Bank; PiC, phosphate carrier; AMPPNP, 5′-adenylyl-β,γ-imidodiphosphate.

solic segment (2, 11). The TPR structure is characterized by the presence of 34-amino acid repeats forming two anti-parallel α-helices separated by a turn, and a triad (TPR clamp domain) has the ability to bind the Hsp90 C-terminal MEEVD motif (7–9). Thus, the TPR clamp domain of Tom70 serves as a docking site for the Hsp70/Hsp90 C-terminal EEVD motifs and consequently forms the multichaperone complexes that constrain a preprotein substrate, which is subsequently transferred to the preprotein-binding site on Tom70 (2, 11). Despite a wealth of studies conducted on the relevance of Tom70·Hsp90 complex formation and its overall role in protein translocation, there is a dearth of information regarding the exact molecular mode of Tom70/Hsp90 interactions. The availability of such information would certainly assist ongoing attempts to elucidate the mechanism by which preproteins are translocated to the mitochondria via the TOM pathway.

In an effort to address this void, we have pursued an experimental strategy that combines chemical cross-linking and mass spectrometry to characterize interactions between the C-terminal domain of human Hsp90 and the cytosolic domain of human Tom70. This multiparametric approach has identified a new contact region within the Hsp90·Tom70 complex, an observation corroborated via isothermal titration calorimetry (ITC) and mitochondrial import assays. The conformational arrangement of this model has been probed by small angle x-ray scattering, hydrogen/deuterium exchange, and mass spectrometry. Our findings in conjunction with published reports on the Hsp90·Tom70 high affinity complex allow us to rationalize a model of chaperone/co-chaperone interactions that may ultimately shed significant insight on the mechanism of preprotein delivery from Hsp90 to Tom70.

Results and Discussion

Chemical Cross-linking and Mass Spectrometry Identify a Novel Region of Hsp90/Tom70 Interaction Confirmed by Isothermal Titration Calorimetry and Mitochondrial Import Assays—To create a reliable model of the C-Hsp90·Tom70 complex, both the isolated (Tom70, Fig. 1*A*, and C-Hsp90, Fig. 1*B*) and associated (C-Hsp90/Tom70, Fig. 1*C*) proteins have been subjected to chemical cross-linking studies. XL-MS data provide distance information by identifying lysine and serine residues that are proximate to each other and have been covalently bound via a bifunctional cross-linking reagent. Because cross-linker molecules impose distance constraints (*i.e.* 30.0 Å for disuccinimidyl suberate (DSS) cross-linker (Cα distance)) on the corresponding proximal lysine residues, the latter allows us to obtain information on both protein tertiary and quaternary structures. The distance constraints explicitly consider DSS spacer length (~11.4 Å), the length of two lysine side chains (~5.5 Å), and the conformational flexibility of cross-linker and protein. The cross-linked patterns for isolated Tom70 (Fig. 1*A*), isolated C-Hsp90 (Fig. 1*B*) and associated C-Hsp90·Tom70 (Fig. 1*C*) are presented.

The chemical cross-linking experiments yield important information on the binding interface between C-Hsp90 and Tom70. The resultant data provide evidence for a novel region of interaction (Fig. 1*C*) apart from that involving the MEEVD motif in C-Hsp90 (12). Specifically, the C-Hsp90 segment spanning Lys-654 to Lys-660 is positioned proximal to several distinct regions in Tom70 extending from Lys-199 to Lys-203, Lys-233, and Lys-319 (Fig. 1*C*). Significantly, the Lys-233 residue in human Tom70 is located within the A7 helix, which is conserved among Tom70 and related Tom71 receptor proteins (Fig. 1*D*) and has been suggested to act as a hinge between the N- and C-terminal domains. This region undergoes a 20° rotation upon binding of the C-terminal Hsp90 MEEVD motif to specific residues in Tom70 spanning the A1 to A5 helices. As a result, helix A7 mediates conformational changes that propagate through the Tom70 C-terminal domain (12, 13), thereby facilitating preprotein binding. In an effort to corroborate our findings, we synthesized a peptide corresponding to the A7-helix region in Tom70 (*i.e.* residues 226–244), encompassing the sequence LLADKVLKLLGKEKAKEKY (as underlined in Fig. 1*D*) to probe specific interactions with C-Hsp90 via ITC analysis.

To characterize the novel interaction sites within the C-Hsp90·Tom70 complex, we conducted ITC experiments employing purified peptides corresponding to the region(s) of interest. Our conventional experimental strategy consisted of titrating the purified peptide into intact protein. Considering the small binding interface of these peptide/protein interactions, the resultant reaction heats and corresponding affinities precluded measurement via conventional ITC methodology. In situations where the binding affinities and/or enthalpies are experimentally inaccessible, alternative ITC protocols have been proposed (14) as a means to acquire the requisite thermodynamic binding parameters. Displacement ITC methods involve titration of a higher affinity ligand into the weaker ligand-bound receptor complex yielding an apparent association constant (K_{app}). In a separate control experiment, one measures the higher affinity binding constant (*i.e.* K_A) in the absence of competitor to determine the low affinity ligand association constant (*i.e.* K_B) as described below.

In this study, we characterized the energetics associated with C-Hsp90·Tom70 complex formation in the absence and presence of excess peptide. The ITC profile monitoring titration of Tom70 into C-Hsp90 (Fig. 2*A*) corroborates the results of previous studies (10) in that complex formation proceeds with a moderately high affinity ($K_A = 2.0 \times 10^6\ \text{M}^{-1}$; $K_d \sim 400$ nM) and is driven by both a favorable enthalpy and entropy. A representative displacement ITC profile (Fig. 2*B*) in which Tom70 is titrated into C-Hsp90 preincubated with excess Tom70 peptide (*i.e.* 200 μM Tom70, LLADKVLKLLGKEKAKEKY) yields an apparent affinity (K_{app}) of $8.3 \times 10^5\ \text{M}^{-1}$ (*i.e.* $K_d \sim 1200$ nM). Invoking the relationship $K_B = [(K_A/K_{app}) - 1] \times 1/[B_T]$, where $[B_T]$ corresponds to the peptide concentration (14), we calculate an estimated peptide binding affinity (K_B) of $1 \times 10^4\ \text{M}^{-1}$ ($K_d \sim 100\ \mu$M). The similarities between ΔH_A and ΔH_{app} (*i.e.* −3.0 kcal mol^{-1}) following correction for the endothermic peptide dilution heats illustrates the difficulty of detecting protein-peptide binding reactions via conventional ITC analysis. The impact of preincubating C-Hsp90 with the Tom70 peptide on the resultant complex dissociation constant (K_d) is illustrated in Fig. 2*C*. Although we considered evaluating peptides from three other regions identified via cross-linking (*i.e.* one in C-Hsp90 and two in Tom70, as depicted in Fig. 1*C*), solubility

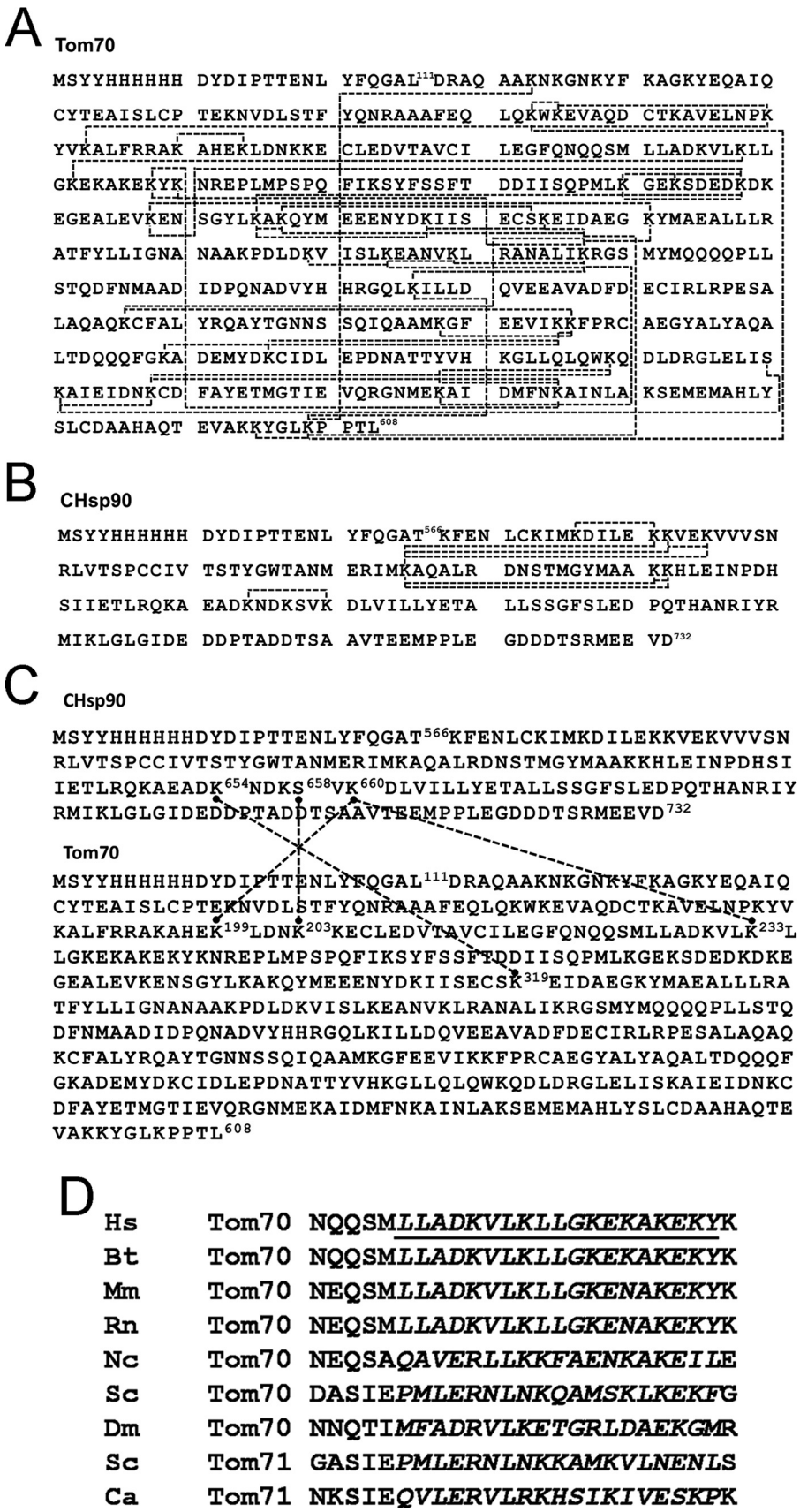

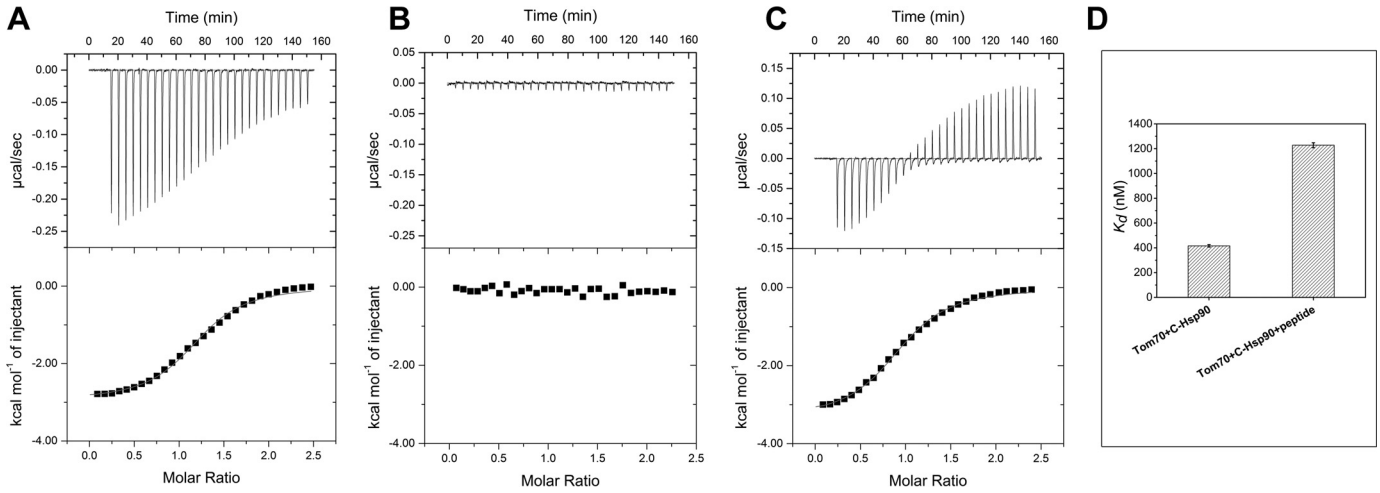

FIGURE 2. **Isothermal titration calorimetry profiles acquired in a buffer system comprised of 20 mM Tris-HCl and 150 mM NaCl (pH 8.0) at 20.0 °C.** *A,* association of full-length Tom70 monomer and C-Hsp90 dimer. *B,* binding of Tom70-peptide and C-Hsp90 demonstrating the lack of a measurable binding profile. *C,* displacement of Tom70-peptide via titration of the Tom70 monomer into C-Hsp90 dimer in the presence of excess Tom70-peptide. *D,* the histograms depict differential dissociation constants in the presence and absence of Tom70-peptide competitor.

issues precluded further investigation (data not shown). The experimentally derived K_d of 0.4 μM corroborates previous studies on the C-Hsp90·Tom70 complex (10) and is typically lower than the binding of other typical TPR domain proteins to MEEVD-containing peptides (*e.g.* $K_d \sim 1–50$ μM) (15). Our findings are therefore consistent with a model that invokes a second Hsp90/Tom70 interface in addition to MEEVD motif binding, both of which may interact cooperatively within the full-length functional complex.

Organelle experiments monitor the effects of Hsp90/Tom70 competitors on the import of polypeptides into mitochondria and thereby provide us with a complementary approach to validate the new region identified via cross-linking studies. We applied this technique by investigating the import of radiolabeled cell-free translated proteins into mitochondria in the absence and presence of peptides. Phosphate carrier (PiC) and Rieske iron-sulfur protein (ISP) are radiolabeled by cell-free translation and their import into isolated HeLa cell mitochondria is monitored by cleavage of their presequences and protection from externally added Proteinase K. The import of PiC to the inner membrane is dependent on Hsp90 and Tom70, whereas that of ISP to the intermembrane space is independent of chaperones and relies on the Tom20 receptor (2). Although the cleaved and protease-protected mature forms are clearly visible in untreated control reactions, reduced levels are observed in reactions treated with valinomycin, which destroys the membrane potential essential for import (Fig. 3*A*). As reported previously (2), the addition of C-Hsp90 competes with full-length Hsp90 and inhibits the import of Tom70-dependent PiC to ~40%, albeit exerting minimal impact on ISP (Fig. 3*A*). Interestingly, a peptide containing the Hsp90 MEEVD motif and Tom70-LLADKVLKLLGKEKAKEKY peptide (see Fig. 1) both exhibit a marginal impact on ISP yet impair PiC import to 57 and 65%, respectively. The lower efficiency of the peptide as a competitor is consistent with the absence of stable folded structures, thereby requiring higher concentrations relative to C-Hsp90 or Tom70. Thus, the A7 helix in Tom70 normally interacts in a folded state with C-Hsp90. Our data nevertheless, confirm that the MEEVD motif in Hsp90 is important for the interaction with Tom70 (2). Furthermore, the data reveal that this newly identified contact between Tom70 (*i.e.* LLADKVLKLLGKEKAKEKY) and the internal region of C-Hsp90 is of comparable functional importance. To further corroborate these results, we explored its impact on import of the Hsp90-TLRQKAEADKNDKSVKDLVILLY peptide (residues 645–667; Fig. 1*C*), representing the interaction site for the Tom70 peptide.

In addition to PiC, we tested another Tom70-dependent inner membrane protein, adenine nucleotide transporter (ANT), which contains no cleaved presequence but is protected from externally added proteinase K (16) (Fig. 3*B*). A scrambled peptide of Hsp90 residues 645–667, DNKDTALAEKLKLY-VKRDQLIVS, was used as a negative control, and has a nonspecific effect on PiC and ANT import (Fig. 3*B*). Addition of C-Hsp90 impairs the import of ANT as well as PiC below that with scrambled peptide, although addition of the Hsp90 peptide containing the MEEVD motif had a weaker effect on ANT (Fig. 3*B*). The Hsp90-TLRQKAEADKNDKSVKDLVILLY internal peptide inhibits import of PiC and ANT to 55 and 53%, respectively. Because the Hsp90 peptides described above represent two separate contacts with Tom70, one might reason that a combination of both peptides should exhibit a greater

FIGURE 1. **Cross-linked patterns for isolated Tom70 (*A*), isolated C-Hsp90 (*B*), and associated C-Hsp90/Tom70 (*C*).** Amino acid sequence of human Hsp90 (residues 566–732) and human Tom70 (residues 11–680) includes N-terminal tags designed for purification purposes. *C,* a region in C-Hsp90, from Lys-654 to Lys-660 that was in close proximity to three different regions in Tom70: from Lys-199 to Lys-203, Lys-233, and Lys-319. *D,* amino acid sequence of the A7 helix of human Tom70. The Lys-233 residue of human Tom70 is located in the A7 helix, which is well conserved among Tom70 and Tom71 and has been previously reported as a potential site of interaction (12). *Hs, Homo sapiens; Bt, Bos Taurus; Mm, Mus musculus; Rn, Rattus novergicus; Nc, N. crassa*; *Sc, Saccharomyces cerevisiae*; *Dm, Drosophila melanogaster*; *Ca, Candida albicans*. One of the peptides studied herein is *underlined*.

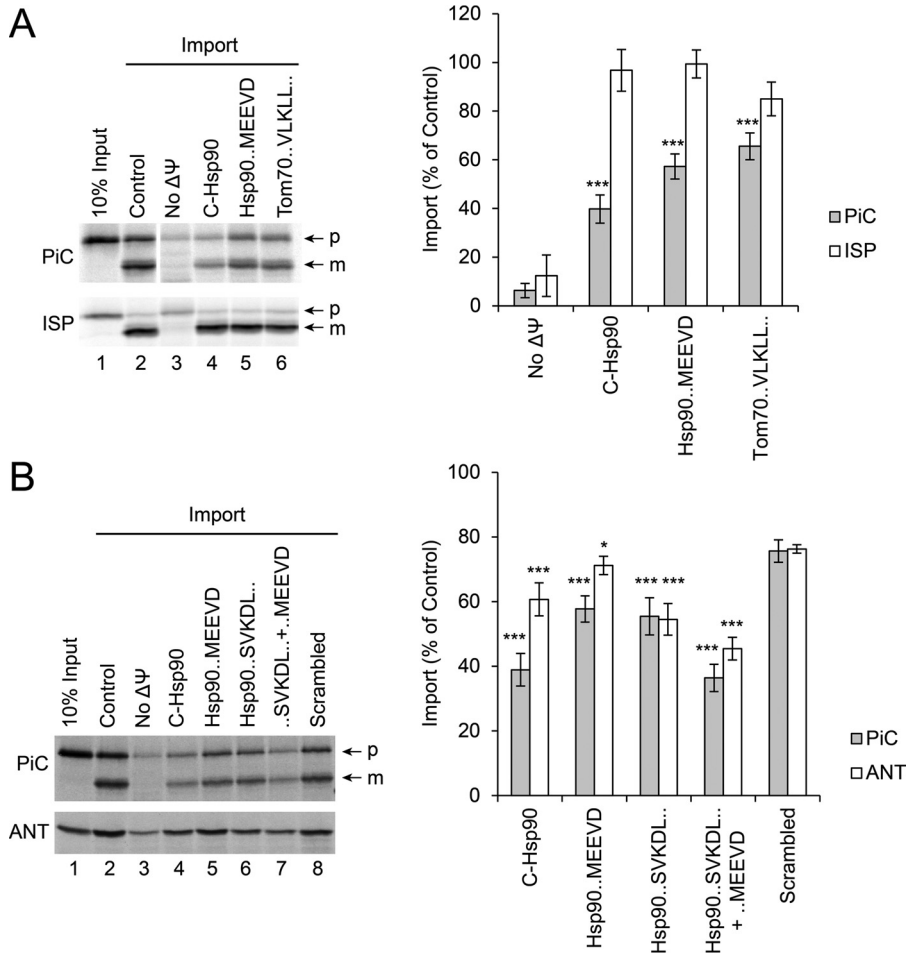

FIGURE 3. **Both Hsp90-Tom70 contacts are required for Tom70-dependent mitochondrial import.** *A, left*, radiolabeled PiC and ISP (*lane 1*) were imported into HeLa cell mitochondria in untreated control reactions, digested with Proteinase K to remove nonspecifically bound protein, and analyzed by SDS-PAGE and autoradiography (*lane 2*). The precursor forms (*p*) were converted to mature forms (*m*) by cleavage of presequences inside mitochondria. Negative control reactions were treated with 1 μM valinomycin to destroy the membrane potential (no $\Delta\Psi$, *lane 3*). Import was assayed upon addition of 20 μM C-Hsp90 or 200 μM of the peptides Hsp90-GYSRMEEVD or Tom70-LLADKVLKLLGKEKAKEKY (*lanes 4* and *5*). *Right*, import was quantified from the amount of the protease-protected mature form and shown as a percentage of that with the untreated control. The standard deviations from the mean of $n \geq 3$ are designated by *error bars*, and *t* test *p* values (***, $p < 0.001$) indicate significant differences relative to the untreated control. *B, left*, radiolabeled PiC and ANT (*lane 1*) were imported into mitochondria as above, in untreated control reactions (*lane 2*), with valinomycin treatment (*lane 3*) and upon addition of 20 μM C-Hsp90, or 200 μM of peptides Hsp90-GYSRMEEVD, Hsp90-TLRQKAEADKNDKSVKDLVILLY, or scrambled sequence DNKDTALAEKLKLYVKRDQLIVS, alone or in combination (*lanes 4–8*). ANT has no cleaved presequence and only its protease-protected mature form is observed. *Right*, import was quantified as described above. The standard deviations from the mean of $n \geq 3$ are designated by *error bars*, and *t* test *p* values (*, $p < 0.05$, ***, $p < 0.001$) indicate significant differences relative to the scrambled peptide control.

inhibitory effect than either peptide alone. Indeed, addition of both peptides impairs PiC import to 36%, a value that is significantly lower than those measured for the individual peptides and comparable with the level observed for C-Hsp90 itself (Fig. 3*B*, *right*). Similar results are obtained for ANT, with the combined peptides more effective than C-Hsp90 alone at blocking import. These findings are consistent with an internal Hsp90-Tom70 contact consisting of peptide regions comprising the interface on both sides. Specifically, Tom70-LLADKVLKLLGKEKAKEKY and Hsp90-TLRQKAEADKNDKSVKDLVILLY compete for the functional interaction at comparable levels. Moreover, the internal contact functions in parallel and of similar importance to the Hsp90 MEEVD motif interaction with the Tom70 TPR clamp domain. We further note that Hsp70 is present in these reactions and may act in Tom70-dependent import by also binding to the TPR clamp domain, but is therefore competed from Tom70 by C-Hsp90 and the MEEVD peptide (2). The internal Hsp90-Tom70 contact is specific to Hsp90, however, the notable block in import by the Hsp90-TLRQKAEADKNDKSVKDLVILLY peptide suggests that it may also affect the Hsp70/Tom70 interaction, most likely by sterically displacing Hsp70 from Tom70. Collectively, these results confirm the existence of additional interactions between C-Hsp90 and Tom70 that complement the MEEVD motif.

On the Conformation of the Hsp90·Tom70 Complex—Our identification and confirmation of a novel binding region necessitates integration of chemical cross-linking, mass spectrometry, and combinatorial modeling to dissect the subunit arrangement of the Hsp90·Tom70 complex. Thus, to improve our understanding of the interaction mechanisms between Hsp90 and Tom70 within the complex, we generated a model based on our findings combined with the results of published studies. Our experimental strategy explicitly incorporates: 1) the successful isolation and purification of both the C-terminal

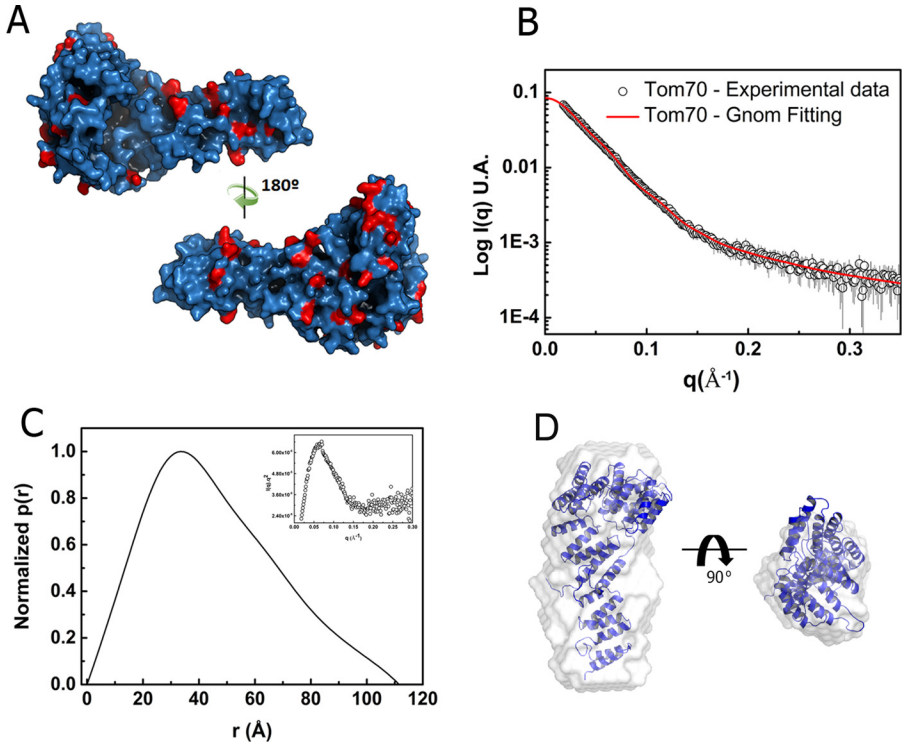

FIGURE 4. **Tom70 model from cross-linking and SAXS data.** *A,* surface representation of Tom70. *Red*, residues modified by DSS in chemical cross-linking as shown in Fig. 1*A*. *B,* experimental scattering curve (*open circles*) and fitting (*red line*). *C, p*(*r*) from GNOM software and Krakty ($q^2 \times I(q)$) plot (*inset*). *D,* SAXS molecular envelope for human Tom70 superposed on the three-dimensional structure derived from molecular modeling using the yeast Tom71 structure as template. See also supplemental Video S1.

portion of human Hsp90 (residues 566–732) and the cytosolic fraction of human Tom70 (residues 111–608) in their native folded conformations (10); 2) the interaction stoichiometry revealing that one Hsp90 dimer binds a Tom70 monomer, forming a tight complex (10); 3) availability of the human Hsp90 crystal structure (residues 293–698, PDB number 3Q6N); and, 4) the crystal structure of yeast Tom71 (residues 107–639) complexed with the yeast Hsp82 C-terminal fragment MEEVD (PDB number 3FP2).

Our objective of elucidating an interaction model for the Hsp90·Tom70 complex represents a multistep process. As an initial attempt, we consider the crystal structure of yeast Tom71 (residues 107–639, PDB number 3FP2), which is 25% identical to human Tom70, in conjunction with the cross-linking results of human Tom70 (residues 111–680; shown in Fig. 1*A*) to construct a structural model of the latter (Fig. 4*A*). The resultant models generated for human Tom70 (Fig. 4*A*) and C-Hsp90 (Fig. 5*A*) satisfy the chemical cross-linking data shown in Fig. 1, *A* and *B*, respectively. As additional support, isolated Tom70 (Fig. 4, *B–D*) and isolated C-Hsp90 (Fig. 5, *B–D*) have been analyzed by small angle x-ray scattering (SAXS). A calculated envelope for the cytosolic domain of Tom70, using DAMMIN software, reveals excellent agreement with the monomeric form and exhibits a high complementarity when superimposed on the three-dimensional envelope model (Fig. 4*D*). The same high complementarity was seen for the three-dimensional envelope model of C-Hsp90 (Fig. 5*D*). Additionally, Kratky plots (insets in Figs. 4*C* and 5*C*) strongly suggested compacted shapes (as expected from their bell-like shape), whereas absence of aggregation was verified by the Guinier approximation (supplemental Fig. S1). Significantly, SAXS experiments validate the conformational models developed from cross-linking assays.

In a subsequent step, we used the results from chemical cross-linking experiments to obtain information on the binding interface between C-Hsp90 and Tom70 as described above and depicted in Fig. 1*C*. We constructed an interaction model by combining these results with the crystallographic structure of human Hsp90 (residues 293–732, structure solved only up to 698) (PDB number 3Q6N). Information on the DSS cross-linked peptides of both Tom70 and C-Hsp90 have been employed to investigate the potential interaction interface of the C-Hsp90·Tom70 complex. The resultant distance constraints guided selection of the most likely subunit arrangement by molecular modeling.

The final model (Fig. 6*A*) is created by invoking the following constraints. 1) Intra-chain Lys cross-links that are in reasonable agreement with those derived from the crystal structure (this study, Fig. 1*C*). 2) Inter-chain cross-links between C-Hsp90 and Tom70 (this study). 3) The MEEVD of C-Hsp90 positioned at the TPR domain using the structure of yeast Tom71 (PDB code 3FP2) as a model. 4) Modeling of the last residues of one monomer of C-Hsp90 in such a manner that it ends at the MEEVD in the TPR domain of Tom70 (this study). The peptide size allowed to establish such a link without breaking any of the above constraints, and, 5) modeling of the last residues in the second monomer of C-Hsp90 allowing for free contacts (this study). In this model, both C-Hsp90 monomers contact Tom70 (Fig. 6*A*).

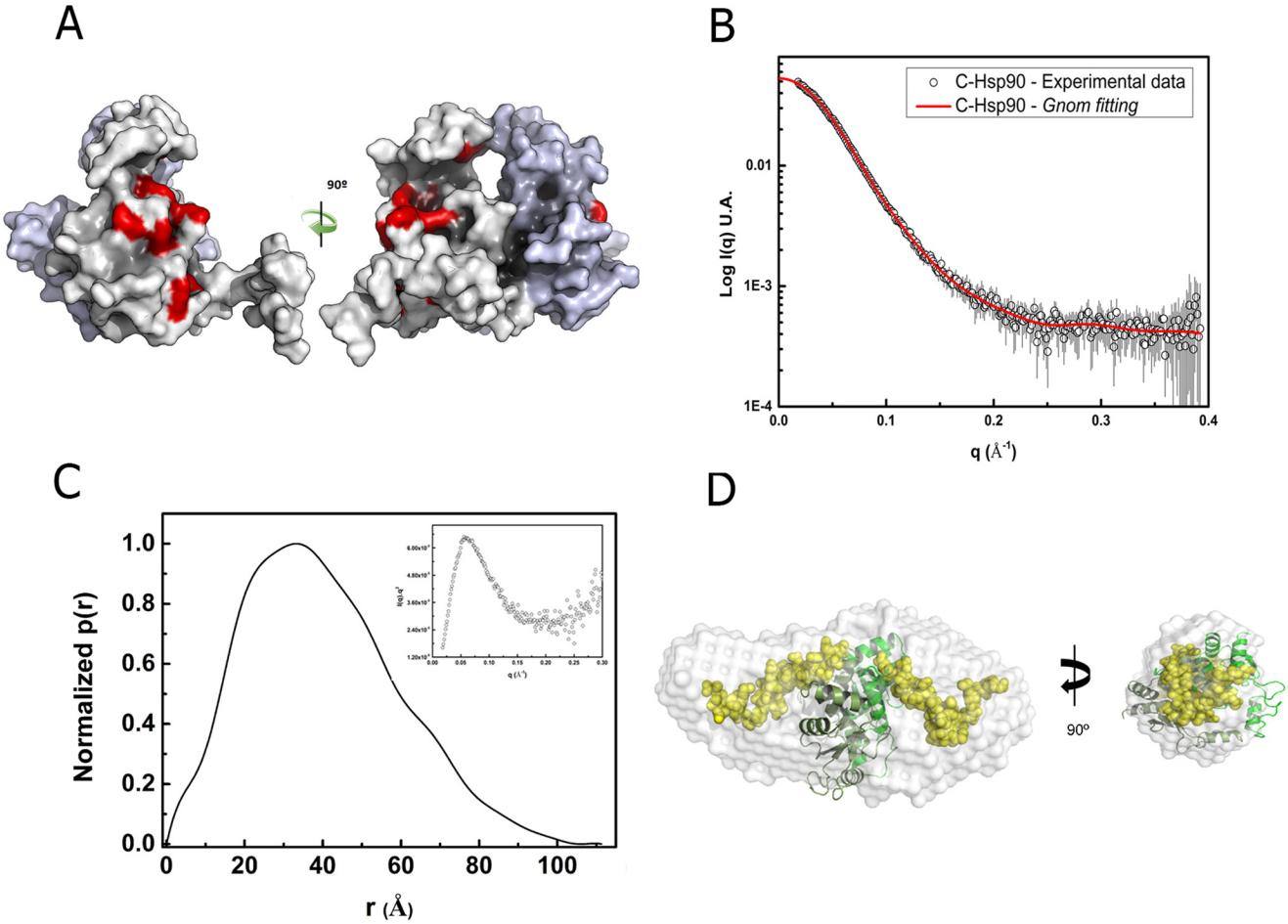

FIGURE 5. **C-Hsp90 model derived from cross-linking and SAXS data.** *A,* dimeric Hsp90 model (monomers are in *gray* and *light blue*). *Red*, DSS-modified residues as shown in Fig. 1*B*. *B,* experimental scattering curve (*open circles*) and fitting (*red line*). *C,* p(r) from GNOM software and Krakty ($q^2 \times I(q)$) plot (*inset*). *D,* molecular envelope from SAXS. See also supplemental Video S2.

To support the final interaction model, we analyzed the C-Hsp90·Tom70 complex by SAXS as illustrated in Fig. 6, *B–D*. Remarkably, the SAXS envelope of the C-Hsp90·Tom70 complex presented intrinsic characteristics of Tom70 due to its elongated shape, but with a higher volume near its central region where the dimer of C-Hsp90 is bound (Fig. 6*D*). Additionally, the Kratky plot (*inset* in Fig. 6*C*) strongly suggested a compacted shape (as expected from its bell-like shape), whereas the absence of aggregation was verified by the Guinier approximation (data not shown). In conclusion, our proposed C-Hsp90/Tom70 interaction model fits properly when superimposed on the envelope obtained by SAXS (Fig. 6*C*), thereby corroborating both the LC/MS-MS and molecular modeling experiments.

Hydrogen/Deuterium Exchange: Insights on the Conformational Changes Accompanying the Interaction of C-Hsp90 and Tom70—HDX-MS experiments have been employed successfully in multiple studies to assess protein dynamics (17–19) and applied in this study to provide information regarding intermolecular dynamics of the dimeric C-Hsp90 when complexed with Tom70. We designed an initial set of experiments to measure the incorporation of deuterium in isolated Tom70 and C-Hsp90 and associated Tom70-MEEVD peptide, Tom70-Scrambled peptide, and Tom70-C-Hsp90. We performed HDX analysis by diluting isolated and associated proteins 15-fold in deuterium solution at different time intervals (10 s to 2 h) and comparing their profile with those of the digestion of undeuterated protein with pepsin under identical conditions.

For isolated C-Hsp90, the digestion of the nondeuterated protein identified 47 peptides representing 90% coverage of the sequence (supplemental Fig. S2). Regions in the dimer interface are protected from exchange, displaying less than 30% deuterium incorporation following 2 h (data not shown). These HDX data are consistent with the crystallographic structure of the chaperone (PDB code 3Q6N).

For isolated Tom70, the digestion of the nondeuterated protein identified 84 peptides representing 84% coverage of the sequence (data not shown). Deuterium incorporation was about 80% in loop regions and from 20 to 60% in α-helical regions (data not shown), as expected from the proposed model for this protein (Fig. 3*A*). Then, the effect caused by the MEEVD peptide, as compared with its scrambled version, used as a control, was investigated. As expected, the MEEVD peptide affected deuterium incorporation but not its scrambled peptide (Fig. 7, *A* and *B*). When considering a level of significance as ±0.5 Da (see Ref. 19), the MEEVD peptide impacted a region similar to that of the interaction in the crystal structure of yeast Tom71 (residues 107–639) complexed with the yeast Hsp82

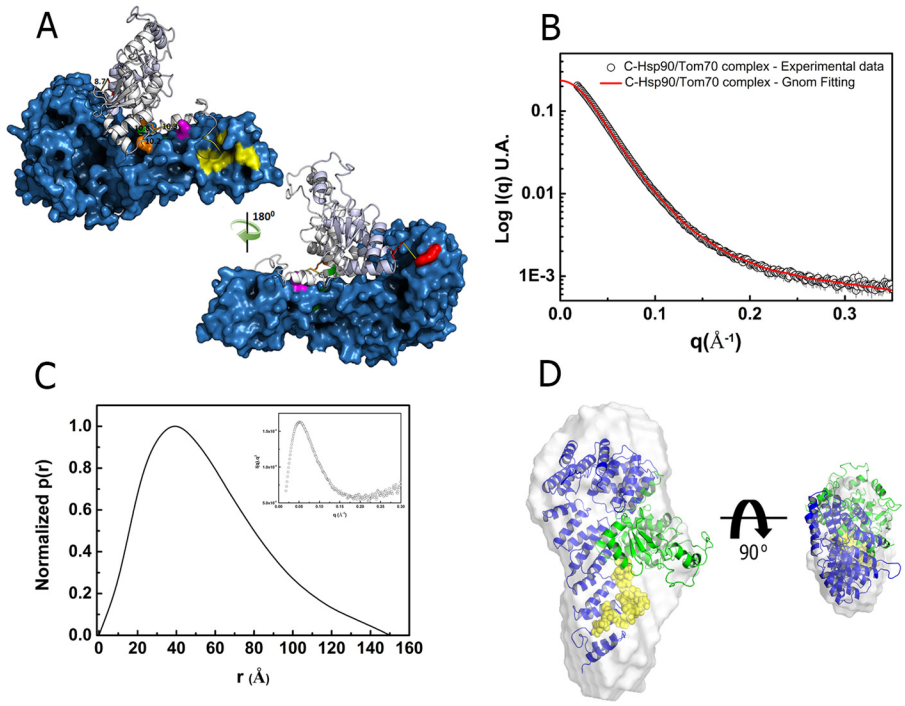

FIGURE 6. **C-Hsp90/Tom70 model from cross-linking and SAXS data.** *A,* C-Hsp90/Tom70 binding interface characterized by XL. The C-Hsp90 and Tom70 binding interfaces appear in *red*, *orange*, *green*, and *magenta*, and the MEEVD motif and its recognition site in *yellow*. *B,* experimental scattering curve (*open circles*) and fitting (*red line*). *C,* $p(r)$ from GNOM software and Krakty ($q^2 \times I(q)$) plot (*inset*). *D,* SAXS envelope for the C-Hsp90/Tom70 superposed on the three-dimensional interaction model proposed in this study. The Tom70 monomer is represented in *blue*, C-Hsp90 dimer in *green*, and the amino acids that are highlighted in *yellow* correspond to the extreme Hsp90 C-terminal regions with unknown tertiary structure. See also supplemental Video S3.

C-terminal fragment MEEVD (PDB number 3FP2) (Fig. 7, *A* and *B*). The regions in Tom70 impacted by the MEEVD peptide are those between 113 and 124 (but has a significant effect on 113–133 but not on 125–133), 163–179, and 190–207 (Fig. 7*A*).

Our subsequent exchange studies evaluated C-Hsp90 deuterium labeling in the presence of Tom70 to identify differences in dynamic conformations of the chaperone within the complex. Peptides at the dimerization interface are not influenced by Tom70 interactions as noted in previous studies (10). Significantly, only 5 regions of C-Hsp90 are impacted by the interaction with Tom70 (Fig. 7*C*) as evidenced by the differential deuterium uptake of free *versus* Tom70-bound C-Hsp90. The strongest effect is that of the peptide TLRQKAEADKNDKSVKDL (residues 645–662), which exhibits a nearly 4 Da reduced mass upon Tom70 binding relative to the free protein (Fig. 7*C*), indicating that amide hydrogens at this peptide are protected from deuterium incorporation. Remarkably, this region overlaps with that identified by DSS chemical cross-linking (Fig. 1*C*) leading to our proposal that it corresponds to an Hsp90 interaction site for Tom70. This region corresponds to the 624–641 segment in yeast Hsp90, which is part of the peptide-(606–645) that is protected by binding of both TPR co-chaperones Cpr6 and Sti1 (21). Thus, we suggest that this may represent an important region of Hsp90 for interaction with TPR co-chaperones in general. C-Hsp90 has also a significant impact on the deuterium profile of Tom70 (Fig. 7*A*). First, C-Hsp90 has a much larger effect on the regions protected by the MEEVD peptide. Second, C-Hsp90 protected other regions not protected by the MEEVD peptide, reinforcing our conclusion that an additional region, or even regions of interaction, was found by our work. Accordingly, the interaction of C-Hsp90 protected the regions containing lysines 199, 203, 233, and 319 (see Fig. 7*A*) identified as being cross-linked to region 654–660 of C-Hsp90 (see Fig. 1*C*) that we claim as a second site of interaction in C-Hsp90 for Tom70. These findings also reinforce the participation of Tom70 helix A7 (Fig. 1*D*) in the interaction with Hsp90.

As concluded here for Tom70, other co-chaperones also have secondary binding sites on Hsp90 (22). Chen and co-workers (23) used mutagenesis to study TPR-containing proteins Hop, Cyp40, FKBP52, and FKBP51 with Hsp90 mutants. Their work indicates that Hop, another TPR co-chaperone that primarily binds to the MEEVD motif, has a secondary interaction with the N-terminal nucleotide-binding domain of Hsp90. Additionally, Hop binds poorly to either Hsp90 mutants deleted of the first 113 residues or with an internal deletion from 381 to 441 residues. On the other hand, FKBP51, an immunophilin protein with PPIase and co-chaperone activities, binds poorly to the Hsp90 T541I single mutant and Hsp90 mutants deleted from residues 548–567 and 601–620 (23). Another study, also using deleted mutants, showed that, besides binding to the MEEVD motif, Hop also binds to the middle domain of Hsp90 (24). Aha1, a co-chaperone that stimulates the ATPase activity of Hsp90, associates with both the N- and C-terminal domains of Hsp90 (25, 26). The co-chaperone p23/Sba1, which inhibits the ATPase activity of Hsp90, binds mainly to the N-terminal but also has binding sites into the middle domain of Hsp90. The crystal structure of yeast Sba1 bound to Hsp90 in the presence of the nonhydrolyzable ATP

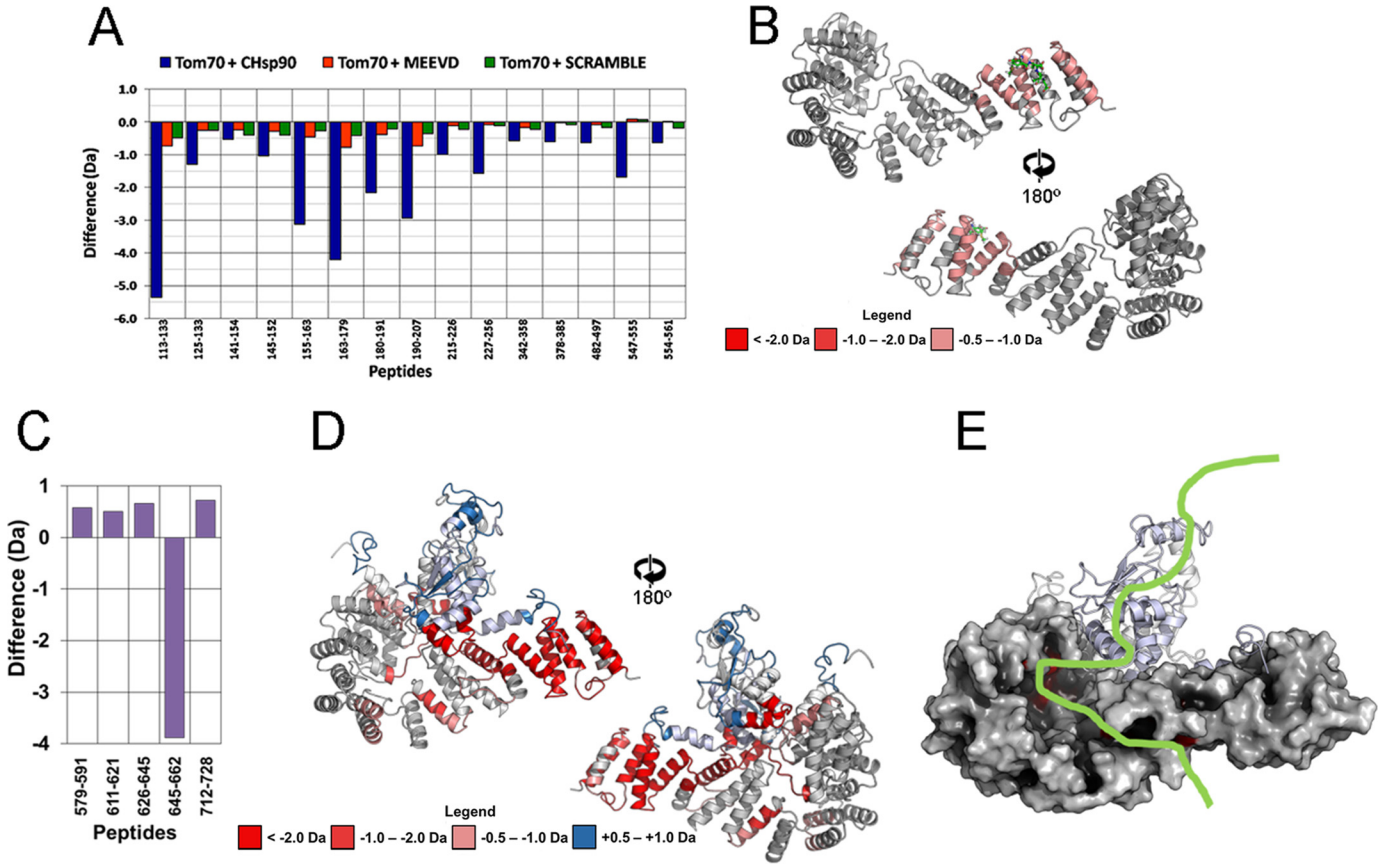

FIGURE 7. **Hydrogen/deuterium exchange experiments.** *A,* deuterium incorporation upon binding (scrambled peptide, *green*; MEEVD peptide, *red*; and C-Hsp90, *blue*) of peptides of Tom70. *B,* regions in Tom70 impacted by the presence of the MEEVD peptide are in *red*. *C,* deuterium incorporation upon binding (Tom70) of peptides of C-Hsp90. Only those with differences >0.5 Da are shown. *D,* C-Hsp90/Tom70 model. The model was built considering the cross-linking and hydrogen/deuterium exchange as explained in the text. Briefly, the model incorporates: 1) the cross-linking results from this work as shown in Fig. 1*C*; 2) the interaction stoichiometry revealing that one Hsp90 dimer binds a Tom70 monomer, forming a tight complex (10); 3) availability of the human Hsp90 crystal structure (residues 293–698, PDB number 3Q6N); 4) the crystal structure of yeast Tom71 (residues 107–639) complexed with the yeast Hsp82 C-terminal fragment MEEVD (PDB number 3FP2); and 5) the hydrogen/deuterium exchange results from this work. See also supplemental Video S4. *E,* C-Hsp90/Tom70/preprotein model, the C-Hsp90/Tom70 model as described in *D*. Residues that appear in *red* are conserved among Tom70 and Tom71 and participate in the pocket dedicated to binding of the preprotein. The *green ribbon* simulates a preprotein bound to C-Hsp90 that would be available to bind within the Tom70 pocket in this model. See also supplemental Video S5.

analogue AMPPNP (27) showed that Hsp90 residues involved with binding are 12–27, 94–125, 151–155, and 376–386.

The conformational arrangement of C-Hsp90 complexed with Tom70 derived from the experimental results presented in this study is summarized in Fig. 7*D* and in a series of videos (supplemental Videos S1–S5), which provides a three-dimensional perspective whereby it is possible to verify the position of C-Hsp90 relative to Tom70 once specific constraints are applied. Furthermore, our structural model advances our understanding of how the protein client is arranged from C-Hsp90 to the cytosolic domain of Tom70. Previous studies (12, 28) have accumulated evidence that a pocket in the C-terminal domain of Tom70 is dedicated to binding of the preprotein. Fig. 7*E* (also in supplemental Video S5) presents a model for the C-Hsp90·Tom70 complex developed from our results in which the residues suggested to comprise the pocket are highlighted in *red*. Although this model is based exclusively on the Hsp90 C-terminal domain, it is evident that a client protein bound to Hsp90 can reach the Tom70 pocket. Moreover, it is entirely plausible that the full-length Hsp90 can bend toward the pocket region to facilitate delivery of the client protein. Finally, the model suggests that one of the MEEVD motifs within dimeric Hsp90 remains free and is conceivably available for other potential interactions.

Concluding Remarks—The interaction between Tom70 and Hsp90 has been investigated by a combined chemical cross-linking/mass spectrometry strategy to identify a novel contact region in the resultant complex. The binding interface has been probed by isothermal titration calorimetry and mitochondrial import assays. Hydrogen/deuterium exchange experiments reveal the site of interaction between C-Hsp90 (corresponding to TLRQKAEADKNDKSVKDLVILLY) and Tom70 is considerably distant from that of the MEEVD motif. These two non-contiguous regions of Hsp90 bind distinct residues within Tom70 and conceivably cooperate in enhancing overall complex affinity. A conformational model of interaction between C-Hsp90 and Tom70 is proposed on the basis of cross-linking and molecular modeling experiments that superimposes neatly on an envelope three-dimensional model generated via SAXS. Our findings elucidate a mode of binding that provides insight into a possible mechanism of preprotein delivery from Hsp90 to Tom70. Collectively, our results complement published studies

and suggest that in addition to the C-terminal MEEVD motif, a second region identified in Hsp90 is integral for the interaction with TPR co-chaperone proteins.

Experimental Procedures

Protein Purification and Folding Characterization—The purification and folding characterization of the Hsp90 C-terminal domain (*i.e.* C-Hsp90, residues 566–732 of Hsp90 AA1–1 or Hsp90-α2), which adopts a dimeric conformation, and the cytosolic portion of Tom70 (residues 111 to 608), which is a monomer, were performed as reported previously (10, 29). Peptides were obtained commercially and further purified to avoid the presence of contaminants.

Chemical Cross-linking Coupled to Mass Spectrometry (XL-MS)—Cross-linking reactions were performed as described previously (30, 31). Briefly, protein preparations in isolated or complex forms were incubated in 20 mM Hepes (pH 7.5) with DSS in a 1:50 ratio (complex:DSS) for 2 h at room temperature and the cross-linking reaction was quenched with 100 mM ammonium bicarbonate (pH 8.0). Reduction and alkylation of cysteine residues were perfomed using dithiothreitol (DTT) and iodoacetamide for 30 min at 60 °C and room temperature, respectively. Each sample was digested by trypsin at 37 °C overnight generating peptides that were analyzed by Q-EXACTIVE (Thermo Fisher Scientific) and SYNAPT G1-HDMS (Waters Corporation) mass spectrometers (32).

Q-Exactive Analysis—Peptides were separated on a nano-LC system (Easy-nLC 1000, Thermo Fisher Scientific) operating in a reverse-phase mode at a flow rate of 300 nl/min using the following mobile phase gradient: 5 to 35% B (50 min), 35–70% B (2 min), and 70% B (8 min). Nano-LC solvents were A (5% CAN and 0.1% formic acid in water) and B (95% CAN and 0.1% formic acid in water). The system was connected to a nano-ESI source coupled to Q-Exactive mass spectrometer (Thermo Fisher Scientific). Mass spectrometry data were acquired continuously over the whole gradient. Each MS scan was acquired in the orbitrap over a mass range of m/z 400–1800 at a resolution of 70,000 (m/z 400), and followed by the 10 data-dependent acquisition mode controlled by XCalibur 2.0 software (Thermo Fisher Scientific). The 10 most intense signals in the mass spectrum were selected for collision-induced dissociation and fragments were detected by Orbitrap at a resolution of 35,000 (m/z 400). Cross-linked peptides were identified using the SIM-XL (33) software program followed by manual validation.

Synapt G1-S HDMS Analysis—Peptides were separated on a nano-LC system (nanoACQUITY UPLC, Waters Co.) operating in a reverse-phase mode at a flow rate of 800 nl/min using the following mobile phase gradient: 3 to 30% B (40 min), 35–70% B (2 min), and 70% B (8 min). Nano-LC solvents were A (0.1% formic acid in water) and B (0.1% formic acid in acetonitrile). The system was connected to a nano-ESI source coupled to a SYNAPT G1-S HDMS mass spectrometer (Waters Corp). MS data were acquired continuously during the whole gradient and each scan was acquired over a mass range of m/z 200–2000, followed by data-dependent acquisition mode and controlled by Masslynx V4.1 software (Waters Co.). The three most intense signals in the mass spectrum were selected for collision-induced dissociation and fragments were detected by time of flight. Cross-linked peptides were identified using the SIM-XL (33) software program followed by manual validation.

Isothermal Titration Calorimetry—Calorimetric binding experiments were performed using a MicroCal VP-ITC instrument (GE Healthcare). Thirty successive 10-μl aliquots of 100 μM human Tom70 monomer were injected into a sample compartment containing 10 μM C-Hsp90 dimer in the absence or presence of 200 μM peptide. All ITC data were acquired in a buffer system comprised of 20 mM Tris and 150 mM NaCl (pH 8.0) at 20 °C. Control experiments consisted of titrating Tom70 monomer into the buffer as a means of correcting for dilution artifacts. The enthalpy accompanying each injection was calculated by integrating the resultant exotherm, which corresponds to the change of power as a function of time. ITC data were analyzed via the MicroCal Origin software program employing a single site binding model and nonlinear least squares analysis of ΔH, K, and n to derive the requisite thermodynamic binding parameters.

Mitochondrial Import—Bovine phosphate carrier (PiC) and *Neurospora crassa* Rieske ISP in pGEM3, and murine adenine nucleotide transporter (ANT2) in pGEM4Z were as described previously (2, 16). The import of radiolabeled cell-free translated proteins into mitochondria was performed as described (34, 35). Briefly, HeLa cells were lysed by passage through a 27-gauge needle. Mitochondria were recovered from the postnuclear supernatant by centrifugation at 12,000 × g for 5 min and resuspended in a buffer containing 20 mM Hepes-KOH, 250 mM sucrose, 80 mM KOAc, 5 mM $MgOAc_2$, 10 mM succinate, 2 mM ADP, and 2 mM DTT (pH 7.5). Cell-free translations of mitochondrial proteins were performed with the TnT-coupled reticulocyte lysate system using SP6 polymerase (Promega) supplemented with [^{35}S]methionine (PerkinElmer Life Sciences), and then terminated with 1 mM methionine and adjusted to 250 mM sucrose. Import reactions contained 25% reticulocyte lysate and 1 mg/ml of mitochondria at 30 °C for 40 to 60 min. Mitochondria were re-isolated and digested with 250 μg/ml of Proteinase K at 4 °C for 10 min, followed by 1 mM phenylmethylsulfonyl fluoride to terminate digestion. Samples were analyzed by SDS-PAGE and PhosphorImager quantitation.

HDX-MS—Proteins were Tom70 and C-Hsp90. Peptides were MEEVD (GYSRMEEVD, in which Y was added to facilitate concentration measurements) and its scramble (GERSDEMVY). Complexes, in which the final concentration of Tom70 was 38 μM, were Tom70·C-Hsp90 (1:10), Tom70·MEEVD (1:10), and Tom70·SCRAMBLE (1:10), were prepared in buffer comprised of 20 mM phosphate and 150 mM NaCl (pH 7.5) and incubated overnight. Hydrogen-deuterium exchange was initiated by a 15-fold dilution of protein or complex in 50 mM phosphate buffer and 150 mM NaCl (pD 7.5) in D_2O at room temperature. Following dilution, the samples were incubated at increasing time intervals (0 s as control and 10 s to 120 min for deuterated experiments). At each time point, the exchange reaction was quenched by adjusting the pH to 2.5 with an equal volume of quench buffer (800 mM guanidine chloride, 0.8% formic acid, 20 mM DTT, pH 2.5). Quenched samples were immediately injected into a nanoACQUITY UPLC Sys-

tem with HDX Technology coupled to SYNAPT G1-S HDMS (Waters Co.) employing electrospray ionization and lock-mass correction (using phosphoric acid). The online digestion was performed via an immobilized pepsin column, 2.0 × 30 mm (Applied Biosystems, USA) for 3 min in H_2O at a flow rate of 40 μl/min. The digestion was incubated at 15 °C inside the temperature-controlled digestion column compartment of the HDX manager. Peptides were trapped and desalted online using an ACQUITY UPLC BEH C18 1.7-μm VanGuard Precolumn (Waters Corp.) at 0 °C. Trapped peptides were eluted into an ACQUITY UPLC BEH C18 1.7 μm, 1 mm × 100-mm column (Waters Co.) equilibrated at 0 °C. Peptides were separated with a 10-min linear acetonitrile gradient (10–40%) containing 0.1% formic acid at a flow rate of 40 μl/min. Mass spectra were acquired in MS^E mode over the m/z range of 50–2000. The analysis of deuterium incorporation was performed by DynamX 3.0 (Waters Corp) followed by manual confirmation. Experiments were performed at least three times.

Small Angle X-ray Scattering—SAXS measurements were acquired using a monochromatic x-ray beam (λ = 1.488 Å) from the D01A-SAXS2 beamline at the Brazilian Synchroton Light Laboratory (LNLS, Brazil). C-Hsp90 (2 mg/ml), Tom70 (2 mg/ml), and C-Hsp90·Tom70 complex (3 mg/ml) samples were prepared in a buffer system composed of 20 mM Tris-HCl and 150 mM NaCl (pH 8.0). Prior to conducting the SAXS experiments, all samples were centrifuged for 15 min at 20,000 × g and 4 °C to remove any potential residual aggregates. The sample-to-detector distance was set as ~1000 mm, resulting in a scattering vector (q) range of 0.02 $Å^{-1} < q < 0.35$ $Å^{-1}$, where the q-vector magnitude is defined as $q = 4\pi \sin\theta/\lambda$ in which 2θ is the scattering angle. Samples were analyzed at 20 °C and placed in 1-mm path length mica cells and the scattering profiles were recorded in 5 successive frames (30 s each) to monitor radiation damage. The buffer contribution in each SAXS profile was subtracted taking into account the attenuation and integrated of the sample using the FIT2D software (36). The Kratky plot is an important tool in SAXS data analysis of proteins in solution. It yields some partial conclusions, without the assumption of any model or approximations (37, 38). For compact proteins, the Kratky plot resembles a bell-like shape, whose peak position mainly depends on the scattering particle radius of gyration. Moreover, the Kratky plot can change it shape if the protein is under an unfolding process, or composed by several flexible regions. The radius of gyration (R_g) was determined using the Guinier approximation (39) and by the indirect Fourier transform methodology using the Gnom package (40). Sample monodispersity was checked by means of the Guinier's law and all studied systems presented here were found to be monodisperse and no aggregation took place over the SAXS curves (data not shown). Gnom program was also used to generate the pair distance distribution function ($p(r)$) and the protein maximum dimension (D_{max}) from scattering profiles. Employing the $p(r)$ function, DAMMIN software (41) was applied to obtain *ab initio* models for C-Hsp90, Tom70, and C-Hsp90·Tom70 complex (dummy atom model) by a simulated annealing optimization routine that yields a best fit to the experimental scattering data. Shapes were reconstructed by averaging a minimum of 10 different *ab initio* models using the DAMAVER package (42). The experimentally derived low-resolution envelopes were superimposed on structures obtained by molecular modeling using the SUPCOMB software (20).

Author Contributions—C. H. I. R. conceived and organized the study; L. M. Z. and T. B. L. collected and analyzed biophysical and functional data on the proteins; M. J. W. conducted mitochondrial import experiments; T. B. S. conducted HDX-MS experiments; C. A. S. A. M., D. P. R., J. C. Y., L. R. S. B., F. C. G., and C. H. I. R. reviewed the results and wrote the paper.

References

1. Neupert, W., and Herrmann, J. M. (2007) Translocation of proteins into mitochondria. *Annu. Rev. Biochem.* **76,** 723–749
2. Young, J. C., Hoogenraad, N. J., and Hartl, F. U. (2003) Molecular chaperones Hsp90 and Hsp70 deliver preproteins to the mitochondrial import receptor Tom70. *Cell* **112,** 41–50
3. da Silva, V. C., and Ramos, C. H. (2012) The network interaction of human 90 kDa heat shock protein Hsp90: a target for cancer therapeutics. *J. Proteomics* **75,** 2790–2802
4. Makhnevych, T., and Houry, W. A. (2012) The role of Hsp90 in protein complex assembly. *Biochim. Biophys. Acta* **1823,** 674–682
5. Jackson, S. E. (2013) Hsp90: structure and function. *Top. Curr. Chem.* **328,** 155–240
6. Li, J., and Buchner, J. (2013) Structure, function and regulation of the hsp90 machinery. *Biomed. J.* **36,** 106–117
7. Steger, H. F., Söllner, T., Kiebler, M., Dietmeier, K. A., Pfaller, R., Trülzsch, K. S., Tropschug, M., Neupert, W., and Pfanner, N. (1990) Import of ADP/ATP carrier into mitochondria: two receptors act in parallel. *J. Cell Biol.* **111,** 2353–2363
8. Das, A. K., Cohen, P. W., and Barford, D.(1998) The structure of the tetratricopeptide repeats of protein phosphatase 5: implications for TPR-mediated protein–protein interactions, *EMBO J.* **17,** 1192–1199
9. Scheufler, C., Brinker, A., Bourenkov, G., Pegoraro, S., Moroder, L., Bartunik, H., Hartl, F. U., and Moarefi, I. (2000) Structure of TPR domain-peptide complexes: critical elements in the assembly of the Hsp70-Hsp90 multichaperone machine. *Cell* **101,** 199–210
10. Gava, L. M., Gonçalves, D. C., Borges, J. C., and Ramos, C. H. (2011) Stoichiometry and thermodynamics of the interaction between the C-terminus of human 90kDa heat shock protein Hsp90 and the mitochondrial translocase of outer membrane Tom70. *Arch. Biochem. Biophys.* **513,** 119–125
11. Fan, A. C., and Young, J. C. (2011) Function of cytosolic chaperones in Tom70-mediated mitochondrial import. *Protein Pept. Lett.* **18,** 122–131
12. Li, J., Qian, X., Hu, J., and Sha, B. (2009) Molecular chaperone Hsp70/Hsp90 prepares the mitochondrial outer membrane translocon receptor Tom71 for preprotein loading. *J. Biol. Chem.* **284,** 23852–23859
13. Li, J., Cui, W., and Sha, B. (2010) The structural plasticity of Tom71 for mitochondrial precursor translocations. *Acta Crystallogr. Sect. F Struct. Biol. Cryst. Commun.* **66,** 985–989
14. Zhang, Y. L., and Zhang, Z. Y., (1998) Low-affinity binding determined by titration calorimetry using a high-affinity coupling ligand: a thermodynamic study of ligand binding to protein tyrosine phosphatase 1B. *Anal. Biochem.* **261,** 139–148
15. Millson, S. H., Vaughan, C. K., Zhai, C., Ali, M. M., Panaretou, B., Piper, P. W., Pearl, L. H., and Prodromou, C. (2008) Chaperone ligand-discrimination by the TPR-domain protein Tah1. *Biochem. J.* **413,** 261–268
16. Bhangoo, M. K., Tzankov, S., Fan, A. C., Dejgaard, K., Thomas, D. Y., and Young, J. C. (2007) Multiple 40-kDa heat-shock protein chaperones function in Tom70-dependent mitochondrial import. *Mol. Biol. Cell* **18,** 3414–3428
17. Engen, J. R. (2003) Analysis of protein complexes with hydrogen exchange and mass spectrometry. *Analyst* **128,** 623–628
18. Wales, T. E., Engen, J. R. (2006) Partial unfolding of diverse SH3 domains on a wide timescale. *J. Mol. Biol.* **357,** 1592–1604

19. Wei, H., Ahn, J., Yu, Y. Q., Tymiak, A., Engen, J. R., Chen, G. (2012) Using hydrogen/deuterium exchange mass spectrometry to study conformational changes in granulocyte colony stimulating factor upon PEGylation. *J. Am. Soc. Mass Spectrom.* **23,** 498–504
20. Kozin, M. B., and Svergun, D. I. (2001) Automated matching of high- and low-resolution structural models. *J. Appl. Crystallogr.* **34,** 33–41
21. Graf, C., Lee, C. T., Eva Meier-Andrejszki, L., Nguyen, M. T., and Mayer, M. P. (2014) Differences in conformational dynamics within the Hsp90 chaperone family reveal mechanistic insights. *Front. Mol. Biosci.* **1,** 4
22. Mayer, M. P., and Le Breton, L. (2015) Hsp90: breaking the symmetry. *Mol. Cell* **58,** 8–20
23. Chen, S., Sullivan, W. P., Toft, D. O., and Smith, D. F. (1998) Differential interactions of p23 and the TPR-containing proteins Hop, Cyp40, FKBP52 and FKBP51 with Hsp90 mutants. *Cell Stress Chaperones* **3,** 118–129
24. Schmid, A. B., Lagleder, S., Gräwert, M. A., Röhl, A., Hagn, F., Wandinger, S. K., Cox, M. B., Demmer, O., Richter, K., Groll, M., Kessler, H., and Buchner, J. (2012) The architecture of functional modules in the Hsp90 co-chaperone Sti1/Hop. *EMBO J.* **31,** 1506–1517
25. Koulov, A. V., LaPointe, P., Lu, B., Razvi, A., Coppinger, J., Dong, M. Q., Matteson, J., Laister, R., Arrowsmith, C., Yates, J. R., 3rd, and Balch, W. E. (2010) Biological and structural basis for Aha1 regulation of Hsp90 ATPase activity in maintaining proteostasis in the human disease cystic fibrosis. *Mol. Biol. Cell* **21,** 871–884
26. Retzlaff, M., Hagn, F., Mitschke, L., Hessling, M., Gugel, F., Kessler, H., Richter, K., and Buchner, J. (2010) Asymmetric activation of the hsp90 dimer by its cochaperone aha1. *Mol. Cell* **37,** 344–354
27. Ali, M. M., Roe, S. M., Vaughan, C. K., Meyer, P., Panaretou, B., Piper, P. W., Prodromou, C., and Pearl, L. H. (2006) Crystal structure of an Hsp90-nucleotide-p23/Sba1 closed chaperone complex. *Nature* **440,** 1013–1017
28. Melin, J., Kilisch, M., Neumann, P., Lytovchenko, O., Gomkale, R., Schendzielorz, A., Schmidt, B., Liepold, T., Ficner, R., Jahn, O., Rehling, P., and Schulz, C. (2015) A presequence-binding groove in Tom70 supports import of Mdl1 into mitochondria. *Biochim. Biophys. Acta* **1853,** 1850–1859
29. Zanphorlin, L. M., Alves, F. R., and Ramos, C. H. (2014) The effect of celastrol, a triterpene with antitumorigenic activity, on conformational and functional aspects of the human 90 kDa heat shock protein Hsp90α, a chaperone implicated in the stabilization of the tumor phenotype. *Biochim. Biophys. Acta* **1840,** 3145–3152
30. da Silva, V. C., Cagliari, T. C., Lima, T. B., Gozzo, F. C., and Ramos, C. H. (2013) Conformational and functional studies of a cytosolic 90 kDa heat shock protein Hsp90 from sugarcane. *Plant Physiol. Biochem.* **68,** 16–22
31. Tiroli-Cepeda, A. O., Lima, T. B., Balbuena, T. S., Gozzo, F. C., and Ramos, C. H. (2014). Structural and functional characterization of the chaperone Hsp70 from sugarcane: insights into conformational changes during cycling from cross-linking/mass spectrometry assays. *J. Proteomics* **104,** 48–56
32. Kahraman, A., Herzog, F., Leitner, A., Rosenberger, G., Aebersold, R., and Malmström, L. (2013) Cross-link guided molecular modeling with ROSETTA. *PLoS ONE* **8,** e73411
33. Lima, D. B., de Lima, T. B., Balbuena, T. S., Neves-Ferreira, A. G., Barbosa, V. C., Gozzo, F. C., and Carvalho, P. C. (2015) SIM-XL: a powerful and user-friendly tool for peptide cross-linking analysis. *J. Proteomics* **129,** 51–55
34. Fan, A. C., Gava, L. M., Ramos, C. H., and Young, J. C. (2010) Human mitochondrial import receptor Tom70 functions as a monomer. *Biochem. J.* **429,** 553–563
35. Fan, A. C., Kozlov, G., Hoegl, A., Marcellus, R. C., Wong, M. J., Gehring, K., and Young, J. C. (2011) Interaction between the human mitochondrial import receptors Tom20 and Tom70 in vitro suggests a chaperone displacement mechanism. *J. Biol. Chem.* **286,** 32208–32219
36. Hammersley, A. P., Svensson, S. O., Hanfland, M., Fitch, A. N., and Hausermann, D. (1996) Two-dimensional detector software: from real detector to idealised image or two-theta scan. *High Pressure Res.* **14,** 235–248
37. Barbosa, L. R. S., Spinozzi, F., Mariani, P., and Itri, R. (2013) Small-angle x-ray scattering applied to proteins in solution. in *Proteins in Solution and at Interfaces*, pp. 49–72, John Wiley and& Sons, Inc., New York
38. Tsutakawa, S. E., Hura, G. L., Frankel, K. A., Cooper, P., and Tainer, K. J. (2007) Structural analysis of flexible proteins in solution by small angle x-ray scattering combined with crystallography. *J. Struct. Biol.* **158,** 214–223
39. Guinier, A., and Fournet, G. (1955) *Small-angle scattering of x-rays.* John Wiley & Sons, Inc., New York
40. Svergun, D. I., Semenyuk, A. V., and Feigin, L. A. (1988) Small-angle-scattering-data treatment by the regularization method. *Acta Cryst. A* **44,** 244–250
41. Svergun, D. I. (1999) Restoring low resolution structure of biological macromolecules from solution scattering using simulated annealing. *Biophys. J.* **76,** 2879–2886
42. Volkov, V. V., and Svergun, D. I. (2003) Uniqueness of *ab initio* shape determination in small-angle scattering. *J. Appl. Crystallogr.* **36,** 860–864

Heat Shock Protein 90 kDa (Hsp90) Has a Second Functional Interaction Site with the Mitochondrial Import Receptor Tom70

Leticia M. Zanphorlin, Tatiani B. Lima, Michael J. Wong, Tiago S. Balbuena, Conceição A. S. A. Minetti, David P. Remeta, Jason C. Young, Leandro R. S. Barbosa, Fabio C. Gozzo and Carlos H. I. Ramos

J. Biol. Chem. 2016, 291:18620-18631.
doi: 10.1074/jbc.M115.710137 originally published online July 8, 2016